

Development of a Qubit Module for Realizing Networks of Superconducting Quantum Processors

Parthorn Ammawat^{1,2}, Piero Chiappina³, and Oskar Painter²

¹*Department of Electrical Engineering, California Institute of Technology, Pasadena, CA 91125*

²*Department of Applied Physics, California Institute of Technology, Pasadena, CA 91125*

³*Department of Physics, California Institute of Technology, Pasadena, CA 91125*

Quantum computers hold the promise of revolutionizing a wide range of scientific fields, including cryptography, drug discovery, and optimization. One prominent platform for constructing a large-scale quantum processor is superconducting quantum circuits. Despite recent developments in increasing the size and complexity of superconducting quantum processors, maintaining high coherence and fidelity control across a large chip remains a key challenge. One approach to scaling is to connect multiple small-scale quantum processors through optical fiber interconnects. Since superconducting qubits do not have a natural interface with optical photons, quantum transducers are needed to interface between microwave and optical photons. Moving forward, it is crucial to develop a qubit module that can efficiently capture microwave photons coming from these transducers. In this work, we design, fabricate, and characterize a qubit module designed to capture incoming microwave photons. Using an existing qubit module as a prototype, we optimize the circuit geometry to achieve better photon absorption efficiency and implement asymmetric superconducting quantum interference devices to improve quantum coherence. The measured results mostly agree well with expectations. The qubit module in this work can be implemented in a future quantum network distributing entanglement across remote superconducting processors.

I. INTRODUCTION

Quantum computing is a rapidly growing area of research, in which the fundamental principles of quantum mechanics, including superposition, interference, and entanglement, are used to develop new computing technologies. The need for quantum computing emerges from the limitations of classical computing; despite its notable progress in the past few decades, it faces significant challenges in solving certain types of problems due to the physical limitations of classical bits, which can exist only in one state (either 0 or 1). Unlike classical computing, quantum computing employs quantum bits or qubits that can exploit quantum mechanical phenomena such as superposition and entanglement, enabling exponential enhancements in computational power for certain tasks. By enabling the solution of problems currently beyond the capability of classical computing, quantum computing has the potential to transform a wide range of fields including cryptography, drug discovery, optimization, and machine learning[1].

Qubits are the fundamental building block of a quantum computer. In order to achieve a quantum computer's advantage over classical computers, or quantum supremacy, multiple qubits are needed. One prominent platform for constructing a multi-qubit quantum processor is superconducting qubits, which are based on superconducting circuit elements. Unlike other platforms, which encode quantum information in natural microscopic quantum systems, superconducting qubits are

macroscopic in size and can be defined through lithography techniques while exhibiting atom-like energy spectra, thus often referred to as artificial atoms[2]. This hardware approach has led to many landmark demonstrations in quantum information science[3].

However, despite recent developments in the increasing size and complexity of superconducting quantum processors, maintaining high coherence and fidelity control across a large chip remains a key challenge[3]. Thus, an alternative scalable technique, building a quantum network, is proposed. In a quantum network, multiple smaller-scale quantum processors are linked together with modular interconnects. Currently, optical photons are the only known means for transferring quantum information over long distances, making them a necessary component for quantum networks. Thus, similar to classical information processing networks, quantum networks have been conceptualized to be connected through optical channels as low-loss, room-temperature links between distant superconducting processors[4]. However, superconducting qubits do not have a natural interface with optical photons since they encode quantum information in microwave-frequency photons, which in turn require operation in millikelvin temperatures to mitigate thermal noise, so a quantum transducer is needed to convert these microwave photons to optical photons for information transmission. Using the scheme described in [9], transducers will enable the realization of networks of superconducting processors with optical fibers as interconnects. If this is successful, the scalability of su-

superconducting quantum processors will be significantly improved.

In the Painter group, the transducer has been previously realized by using piezo-optomechanics, which uses acoustic phonons as intermediate excitations in the conversion process[5]. In addition, recent works from the Painter group have successfully demonstrated non-classical microwave-optical photon pair generation and entangled optical and microwave photonic qubits from these transducers, which is a key ingredient to utilize these transducers to connect remote superconducting qubits[4, 6]. Henceforth, to realize the remote entanglement schemes proposed in [7], it is critical to develop a superconducting qubit module that can efficiently capture microwave photons coming from the transducer.

This project focuses on achieving this photon capture by using the scheme from [8], where photon absorption is mediated by a strong time-dependent microwave-frequency pulse. Ultimately, if this is successful, it will realize information sharing between optically connected remote superconducting qubits in a quantum network, which will in turn enable distributed quantum information processing.

II. DEVICE DESIGN

In the Painter group, a prototype qubit module has been fabricated and characterized prior to this work. The device is comprised of aluminum microwave circuits on a high-resistivity silicon substrate. These superconducting qubits are made possible with the Josephson junction, which is comprised of an insulator between two superconductors. When this Josephson junction is connected to a large capacitor, it exhibits atom-like energy levels, and the ground and first excited state of this circuit can be utilized as a qubit. This type of qubit is known as the transmon. The main components of a qubit module include a communication resonator for capturing microwave photons, a drive line for qubit operations, a readout resonator for measuring the state of the qubit, and a transmon qubit which consists of a metal island connected to the ground plane by Josephson junctions (Fig. 1). The qubit is coupled capacitively to both of the resonators via claws at the voltage maxima of the resonators.

However, the prototype qubit chip can be further optimized for better performance in two main aspects: the photon absorption efficiency, mediated by a system of coplanar microwave resonators, and the quantum coherence, governed by a superconducting quantum coherence device (SQUID).

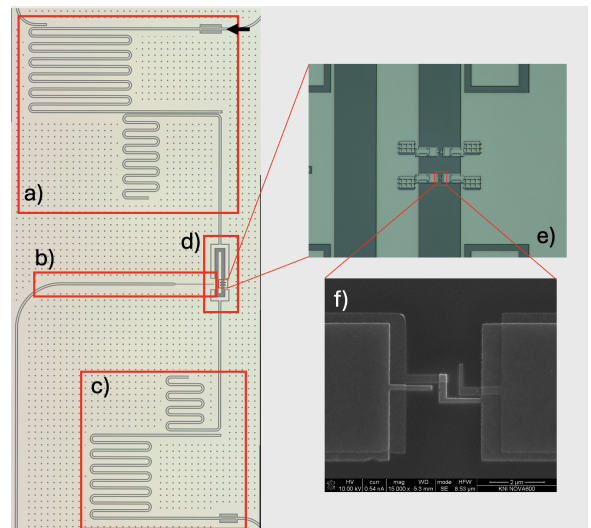


FIG. 1: Layout of the qubit module. The main components are a) a communication resonator, b) a qubit drive line, c) a readout resonator, d) a qubit, e) a superconducting quantum interference device (SQUID), and f) a Josephson junction. The arrow indicates where the microwave photons coming from a transducer will get absorbed by the communication resonator.

A. Coplanar Microwave Circuits

The geometry of the microwave circuits defines the frequencies of the qubit-resonator system, including the readout frequency, the communication frequency, the coupling between the qubit and the resonators, and the qubit shunt capacitance. The communication frequency is chosen to match the frequency of the photons coming from a transducer, and the readout frequency and coupling is selected to minimize interference with the qubit while maximizing the readout signal. The coupling between the qubit and the communication resonator is selected to maximize the photon absorption rate.

These systems can be simulated with a commercial 2D microwave circuit simulation software Sonnet by defining the desired geometry and sweeping the parameters to get the targeted responses. The coupling and shunt capacitance can be optimized by adjusting the qubit and claw geometry (Fig. 2a), and the resonator frequencies can be controlled by adjusting the lengths of the resonators (Fig. 2b).

B. SQUIDs

The quantum coherence of the qubit is governed by a SQUID, a superconducting loop consisting of two Josephson junctions in parallel (Fig. 1e), which enables fre-

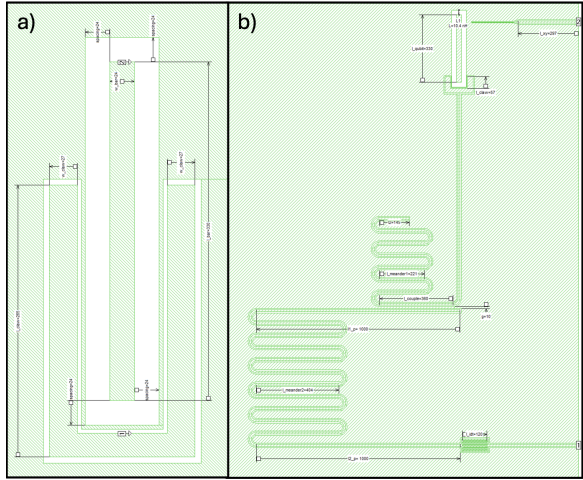


FIG. 2: Simulation setups in Sonnet a) for adjusting the qubit and claw geometry and b) for adjusting the resonator lengths.

quency control of the qubit using an applied magnetic flux[2]. The prototype qubit utilizes a symmetric SQUID, where the Josephson junctions have an identical area (Fig. 3a), which, in turn, enables a large frequency tunability (Fig. 3b). However, since the sensitivity to random magnetic flux noise depends directly on the slope of the spectrum at any working point, if the desired qubit frequency does not land exactly at any of the maxima (red dots in Fig. 3b) due to fabrication uncertainty, the qubit frequency can be greatly affected by magnetic flux noise, significantly decreasing the coherence time of the qubit due to frequency jitter. One solution to this issue is to replace a symmetric SQUID with an asymmetric SQUID, in which the two junctions are made asymmetric in area (Fig. 3c)[10]. As shown in the spectrum in Fig. 3d, the sensitivity of the qubit to magnetic flux can be considerably decreased, corresponding to increased coherence, with a tradeoff of smaller tunability. By using the equations governing the dynamics of an asymmetric SQUID, qubits with the desired frequency range can be designed.

III. DEVICE FABRICATION

The CAD file of a qubit chip is shown in Fig. 4a. There are 4 qubits on one chip, with the spacing between the qubits large enough to avoid any interference between them. The geometries of the qubits and resonators are also designed such that the frequencies of the qubits and resonators are swept by a fixed small amount (50 MHz for qubit transition frequency, 40 MHz for readout resonator frequency, and 20 MHz for communication resonator frequency), and the devices are ordered such

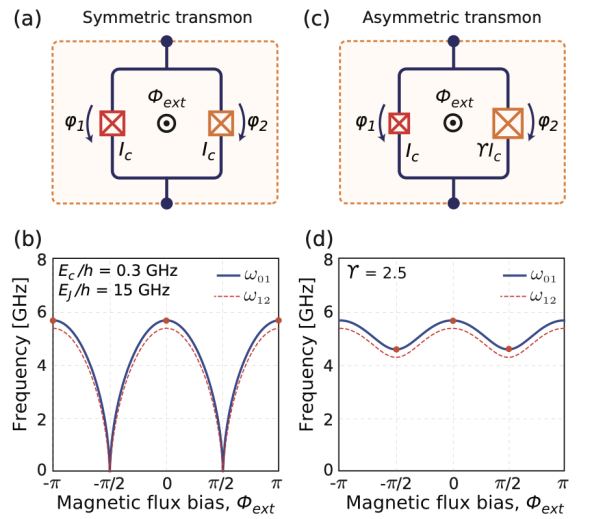


FIG. 3: Circuit representations of a SQUID and corresponding qubit transition frequencies for the two lowest energy states as a function of applied magnetic flux for (a-b) a symmetric SQUID and (c-d) an asymmetric SQUID. (Krantz, et al., 2019)

that the frequency difference between any two adjacent devices is maximized.

The device is fabricated on a high-resistivity silicon substrate. In the Painter lab, we use aluminum (Al) as the superconductor for the qubit module. To create the ground plane, the first layer that defines the geometries of the qubits and resonators, we use ZEP520A as the electron beam resist and the EBPG5200 electron beam lithography system to define the pattern. We then deposit 120 nm of Al to complete the first layer. The next step is to fabricate the Josephson junctions. In this step, a bilayer resist (PMMA/MMA) is used to create an undercut region (red region in Fig. 4b), which is then used with an angled deposition of Al to fabricate the Josephson junctions. During the angled deposition, there are 3 main steps: first angled deposition (from the left in Fig. 4b) to create the first leg of the junctions, oxidation to generate a thin insulating layer for the junctions, and second angled deposition (from the top right in Fig. 4b) to construct the second leg of the junctions. Lastly, using a process similar to that for the junctions, small Al pads connecting the legs of the junctions to the ground plane are deposited to ensure good electrical connections.

IV. CHARACTERIZATION

We characterize the qubits to determine their parameters, including the frequencies of the resonators, the qubits' transition frequency and shunt capacitance, the

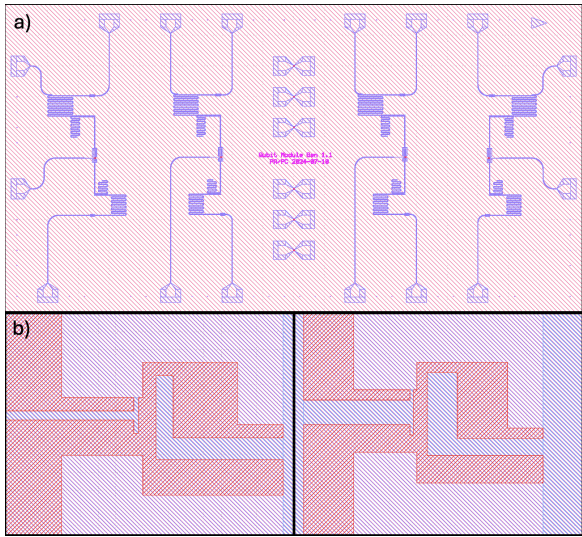


FIG. 4: CAD file of a qubit chip. The figure shows a) the overview of the chip layout and b) the Josephson junctions. Blue indicates the junction pattern and red indicates the undercut region for angled evaporation.

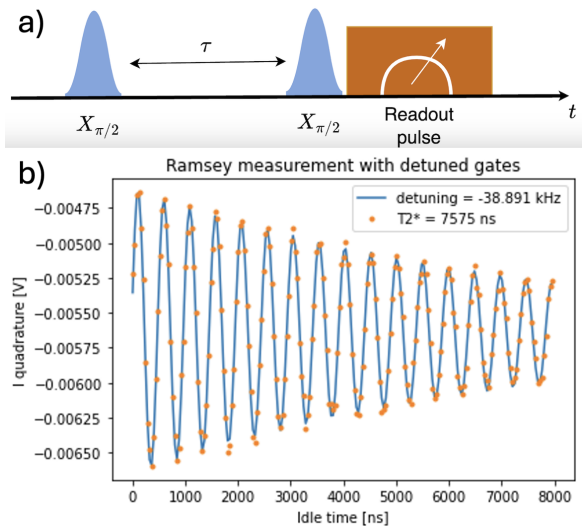


FIG. 5: The Ramsey interferometry for measuring T_2^* of the qubit: a) The pulse sequence and b) The measured result and fit for calculating T_2^* .

sweet spots where the qubits are least sensitive to magnetic flux noise, the coupling between the qubits and communication resonators (g) for estimating photon absorption rate ($\propto g^2$), and the qubits' quantum coherence quantified by dephasing time (T_2^*).

First, an external microwave source is used to drive the readout resonators of each qubit, and the reflected signals are measured to find the resonant frequencies. The frequency of the readout resonator is then probed for varying external applied magnetic fields, which tune

the qubit transition frequency and, in turn, shift the resonator's frequency due to the resonator's dispersive coupling to the qubit. The sweet spots are at the plot's turning points between the resonance frequency and external magnetic field.

Next, a two-tone spectroscopy is used to find the qubit transition frequency and shunt capacitance. The two-tone spectroscopy is performed by applying a microwave tone that directly drives the qubit and observing the frequency of the readout resonator with a second microwave tone. When the qubit driving frequency matches one of its transition frequencies, the frequency of the readout resonator will be shifted. Using an appropriate drive power, this measurement can excite transition frequencies corresponding to the qubit's transitions from its ground to the first excited state and ground to the second excited state. This allows for the determination of both the qubit frequency and shunt capacitance.

Using a similar technique on the communication resonators, the shift in resonators' frequencies when the qubits are excited can be measured, after which the coupling between the qubits and communication resonators can be calculated.

Finally, T_2^* of the qubits can be determined by using the Ramsey interferometry (Fig. 5), which is performed as follows: the qubit is prepared in a superposition state between the ground and first excited state using an appropriate microwave drive pulse, then the qubit is allowed to freely evolve for a time τ , after which a second drive pulse is applied and the qubit state is measured[2]. By varying the free evolution time τ , the result of this measurement is an exponentially decaying sinusoidal function (Fig. 5b) with a characteristic time T_2^* .

V. RESULTS

The fabricated chip is shown in Fig. 6 with the dimensions of the devices matching the design well. The

Qubit	f_{ge} (GHz)	α (MHz)	f_{RR} (GHz)	f_{comm} (GHz)
1	6.01-7.01	324	7.68	5.00
2	5.88-7.15	329	7.72	5.10
3	5.96-7.15	329	7.70	5.05
Target	6.00-7.00	350	7.69-7.73	4.99-5.07

TABLE I: Measured qubit frequency range and relevant frequencies at the upper sweet spots of the qubits. f_{ge} : qubit transition frequency from ground to first excited state, α : qubit's anharmonicity, f_{RR} : readout resonator's resonant frequency, f_{comm} : communication resonator's resonant frequency.

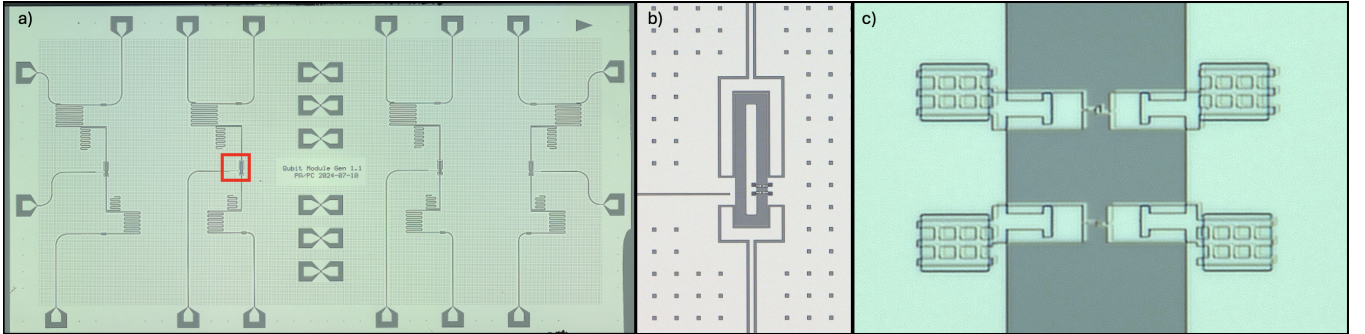


FIG. 6: The fabricated chip under an optical microscope: a) the overview of the chip, b) a zoomed-in image of a qubit (red rectangle in a)), and c) a SQUID loop.

Resonator	1	2	3	Target
κ (kHz)	228	414	607	3000

TABLE II: Measured linewidths (κ) of the readout resonators.

chip was then wire bonded to a PCB board specifically designed to connect the ports on the chip to external coaxial cables. For qubit 4, the resonances could not be found, so the frequencies could not be determined. This could result from poor cable connections to the chip or broken traces on the chip. The measured frequencies and readout resonator linewidths are displayed in Table I and II, respectively. The frequencies, including the qubit transition frequency, readout resonator frequency, and communication resonator frequency, align with what was expected from the design. However, the readout resonator linewidths turned out to be much smaller than the target. From the measured dispersive shift of the communication resonators, the coupling between the qubit and communication resonator was calculated to be $g = 156$ MHz, which is larger than that of the prototype qubit with $g = 137$ MHz. Lastly, the measured T_2^* of each qubit at different qubit frequencies are shown in Fig. 7. Compared to the values from the prototype qubit, at the same frequency, T_2^* is significantly improved for every qubit. In addition, the average T_2^* was calculated to be $2.86 \mu\text{s}$, which is also larger than the average T_2^* of the prototype qubit ($<1 \mu\text{s}$), and T_2^* never falls below $1 \mu\text{s}$ at any frequency for this qubit module.

VI. CONCLUSION

The relevant frequencies of this qubit module are all in line with the design. Furthermore, the quantum coherence of the qubits is significantly improved, as seen from the increase in T_2^* by approximately a factor of

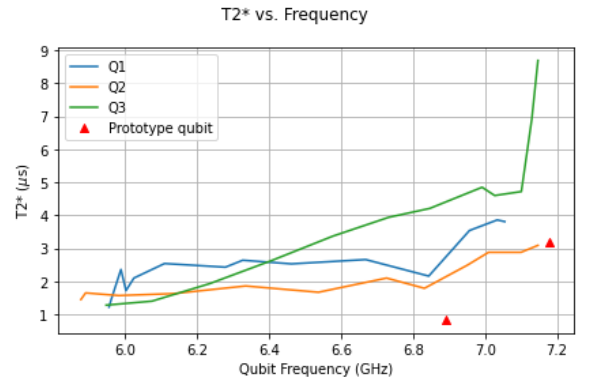


FIG. 7: The measured T_2^* of the qubits at different qubit frequencies. The maximum, minimum, and average values are $8.69 \mu\text{s}$, $1.22 \mu\text{s}$, and $2.86 \mu\text{s}$, respectively. The red triangles are the data points from the old prototype qubit module.

3 on average, and the photon absorption rate also improves by about 30%. However, the readout resonator linewidths are much smaller than expected, increasing the readout time and adversely affecting the readout fidelity. The next steps will be to first address this problem by adjusting the readout resonators' design to increase the linewidths. Once the qubit module becomes good enough, we can move on to integrate a qubit module with a transducer to realize efficient capture of microwave photons coming from a transducer. Ultimately, if this is successful, the two-node remote entanglement experiment can be set up, by entangling two optical photons coming from two of these qubit-transducer systems, demonstrating the first step towards realizing a quantum network.

Acknowledgments

I would like to thank Professor Oskar Painter for giving me this opportunity to be a part of this project and

Qubit	f_{ge} (GHz)	α (MHz)	f_{RR} (GHz)	f_{comm} (GHz)
1	5.96-6.95	350	7.69	4.99
2	6.00-7.00	350	7.73	5.07
3	6.04-7.05	350	7.71	5.03
4	6.08-7.10	350	7.75	5.11

TABLE III: The qubits' target parameters.

Piero Chiappina for being an amazing mentor giving me helpful advice and guiding me throughout this project. I would also like to thank David Lake for helping me with measurements and everyone else in the Painter group for welcoming me. Finally, I would like to thank the Nellicie Bergen and Adrian Foster Tillotson SURF Fellowship, the Institute for Quantum Information and Matter (IQIM), and Amazon Web Services (AWS) for the funding, and the Kavli Nanoscience Institute (KNI) at Caltech for the nanofabrication facilities.

Appendix A: Qubit Parameter Sweeps

The qubits' targeted parameter sweeps are shown in Table III.

Appendix B: Asymmetric SQUID Design

The Hamiltonian of a single Josephson junction with energy E_J (proportional to the area of the junction and can be determined experimentally) is given by

$$H = 4E_C n^2 + 2E_J \cos \phi, \quad (B1)$$

where E_C is the total capacitive energy stored in the system, n is the excess number of Cooper pairs on the qubit's island, and ϕ is the gauge-invariant phase of the junction. The frequency of the qubit is then given by

$$\hbar\omega_q = \sqrt{8E_J E_C} - E_C. \quad (B2)$$

If the junction is replaced by a symmetric SQUID loop with total energy E_J and an applied external magnetic flux ϕ_e , the Hamiltonian becomes

$$H = 4E_C n^2 + 2E_J |\cos \phi_e| \cos \phi, \quad (B3)$$

with an effective Josephson energy $E'_J = E_J |\cos \phi_e|$. The qubit frequency now is given by

$$\hbar\omega_q = \sqrt{8E_J E_C |\cos \phi_e|} - E_C. \quad (B4)$$

If the Josephson junctions are not identical such that $E_{J1}/E_{J2} = \gamma$, for an asymmetric SQUID, the Hamiltonian can be expressed as

$$H = 4E_C n^2 + 2E_{J\Sigma} \sqrt{\cos^2 \phi_e + d^2 \sin^2 \phi_e} \cos \phi, \quad (B5)$$

with

$$E_{J\Sigma} = E_{J1} + E_{J2}, \quad d = \frac{\gamma - 1}{\gamma + 1} \quad (B6)$$

Similar to the symmetric case, the qubit frequency is now given by [2]

$$\hbar\omega_q = \sqrt{8E_{J\Sigma} E_C \sqrt{\cos^2 \phi_e + d^2 \sin^2 \phi_e}} - E_C. \quad (B7)$$

In this project, we chose $\gamma = 6.87$ and $E_{J\Sigma} = h \cdot (19.3 \text{ GHz})$ such that the qubit frequencies at the upper and lower sweet spots are 7 GHz and 6 GHz, respectively.

-
- [1] Patil, Shreya U. "Quantum Computing: Why Do We Need It ?" Medium, Geek Culture, 8 Mar. 2023, medium.com/geekculture/quantum-computing-why-do-we-need-it- 7710d 5d d 9682.
 - [2] Krantz, P., et al. "A Quantum Engineer's Guide to superconducting qubits." *Applied Physics Reviews*, vol. 6, no. 2, 1 June 2019, https://doi.org/10.1063/1.5089550.
 - [3] Kjaergaard, Morten, et al. "Superconducting qubits: Current State of Play." *Annual Review of Condensed Matter Physics*, vol. 11, no. 1, 10 Mar. 2020, pp. 369–395, https://doi.org/10.1146/annurev-conmatphys-031119-050605.
 - [4] Meesala, Srujan, et al. Quantum Entanglement between Optical and Microwave Photonic Qubits, 2023, https://doi.org/https://doi.org/10.48550/arXiv.2312.13559.
 - [5] Mirhosseini, Mohammad, et al. "Superconducting qubit to optical photon transduction." *Nature*, vol. 588, no. 7839, 23 Dec. 2020, pp. 599–603, https://doi.org/10.1038/s41586-020-3038-6.
 - [6] Meesala, Srujan, Steven Wood, et al. Non-Classical Microwave-Optical Photon Pair Generation with a Chip-Scale Transducer, 2023,

- [https://doi.org/https://doi.org/10.48550/arXiv.2303.17684.](https://doi.org/https://doi.org/10.48550/arXiv.2303.17684)
- [7] Zhong, Changchun, et al. "Microwave and optical entanglement for quantum transduction and Network." Quantum 2.0 Conference and Exhibition, 2022, <https://doi.org/10.1364/quantum.2022.qth4a.2>.
- [8] Kurpiers, P., et al. "Deterministic quantum state transfer and remote entanglement using microwave photons." *Nature*, vol. 558, no. 7709, June 2018, pp. 264–267, <https://doi.org/10.1038/s41586-018-0195-y>.
- [9] Pechal, M., et al. "Microwave-controlled generation of shaped single photons in circuit quantum electrodynamics." *Physical Review X*, vol. 4, no. 4, 17 Oct. 2014, <https://doi.org/10.1103/physrevx.4.041010>.
- [10] Hutchings, M.D., et al. "Tunable superconducting qubits with flux-independent coherence." *Physical Review Applied*, vol. 8, no. 4, 12 Oct. 2017, <https://doi.org/10.1103/physrevapplied.8.044003>.